CHAPTER 7:
MEASUREMENTS IN THE TEST BEAM

7.1 Overview of experiment E896

Experiment E896 is a heavy-ion fixed target experiment measuring ^{197}Au+^{197}Au collisions at energy of *11.6 GeV* per nucleon [ref. 7.1]. The experiment took place at the Alternating Gradient Synchrotron accelerator (AGS) at Brookhaven National Laboratory. The main physics motivation for this experiment is the search for the H_0 dibaryon, an exotic 6-quark state, which has never been measured. In addition, the experiment has a high sensitivity for short lived particles which complements the previous AGS heavy-ion strangeness measurements by measuring particles such as Λ, $\overline{\Lambda}$ and Ξ^- in Au+Au collisions. This high sensitivity for short-lived particles is achieved by using an array of STAR/SVT Silicon Drift Detectors positioned near the interaction target for charged particle tracking. In this thesis, the performance of the Silicon Drift Detectors in E896 is presented and discussed, in particular through data measured during the January 1997 beam time, which constituted the first integrated test of the SVT system. Detectors were coupled to their corresponding front-end electronics, and data were processed through the respective Readout and Data-Acquisition systems.

7.1.1 Physics goals of experiment E896

The aim of experiment E896 [ref. 7.1, 7.2] is to study exotic particles and the possible formation of a new state of nuclear matter under the extreme

conditions of temperature and density that are created in relativistic heavy-ion collisions. The main physics motivation for this experiment is the search for the short-lived weakly decaying H_0 dibaryon.

Up to now, particles have only been observed in triplet quark states *qqq* or $\overline{qqq}$ (baryons), or doublet $q\bar{q}$ states (mesons). The states are in accordance with the standard model, however Quantum Chromodynamics imposes no specific limitation on the number of quarks forming a hadronic state other than the generation of a color singlet state. Therefore, it was proposed that a colorless six-quark state "*uuddss*", named H_0, with baryon number $B=2$, spin-parity $J^{\pi}=0^{+}$ and strangeness $S=-2$ may exist [ref. 7.3]. It was postulated that it might have sufficient color-magnetic binding to be stable against strong decays, and therefore would decay weakly with a measurable lifetime. This particle is the simplest and most plausible of the multi-quark states, originally derived from the MIT bag model [ref. 7.4]. The existence of the H_0 is in a sense a prerequisite for the existence of heavier strange matter states, as they are unlikely to be stable if the simpler, more symmetric and lighter "*uuddss*" six-quark is not. The possible existence of heavier strange matter has many physical and cosmological consequences such as a signature for a phase transition in the early phases of the universe, an explanation for dark or missing matter and as a possibility for the core matter of neutron stars [ref. 7.5].

Many models predict different masses for the H_0 dibaryon [ref. 7.6, 7.7], therefore a measurement of the H_0 mass may rule out some models, and place substantial constraints on allowed parameters in other models. As shown in Table 7.1, the predicted H_0 decay modes, branching fractions and lifetimes depend on the mass of the dibaryon. Figure 7.1 summarizes the various mass predictions for the H_0 dibaryon. Although the models are very different in philosophy, they favor an H_0 dibaryon mass in the range $2.0 \leq M \leq 2.3$ GeV/c^2.

Table 7.1

Mass (GeV/c^2)	decay channel	decay mode	branching fraction (%)	lifetime
$2.23 \le M$	$\Lambda + \Lambda$	strong	100	$\sim 10^{-23}$s
$2.13 \le M \le 2.23$	$\Sigma^- + p$	weak, $\Delta S=1$	~30	≥100 ps
	$\Lambda + p + \pi^-$	weak, $\Delta S=1$	~13	
	$\Lambda + n$	weak, $\Delta S=1$	~16	
	$\Sigma^0 + n$	weak, $\Delta S=1$	~34	
	$\Lambda + n + \pi^0$	weak, $\Delta S=1$	~7	
$2.06 \le M \le 2.13$	$\Lambda + n$	weak, $\Delta S=1$	100	~100 ns
$1.88 \le M \le 2.06$	N + N	weak, $\Delta S=2$	100	~10 days
$M \le 1.88$	stable			

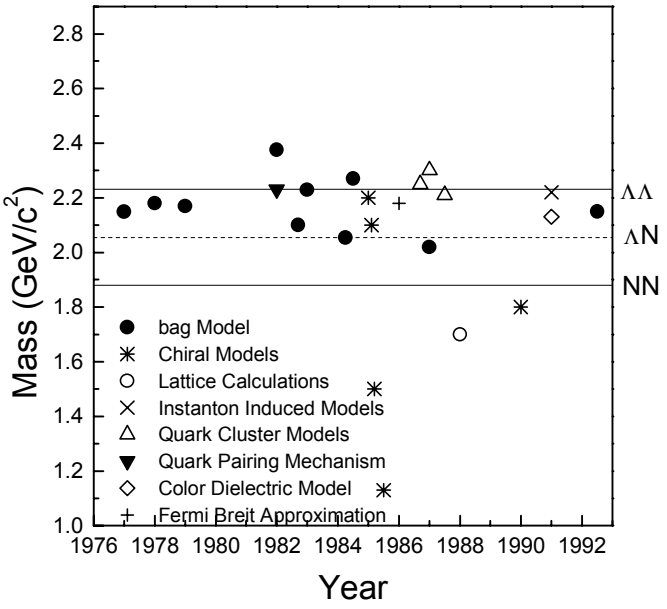

Figure 7.1: *Masses of H_0 dibaryons predicted by different models versus the year that the prediction was described.*

Several previous experiments searched for H_0's but with no compelling success [ref. 7.8, 7.9, 7.10]. There is no conclusive evidence confirming or denying the existence of the H_0. Recently though, two claims of the existence of the H_0 dibaryon were made. In the BNL-AGS experiment 888 [ref. 7.11], two possible candidates of the $H_0 \to \Lambda + n$ channel were observed in p+^{195}Pt collisions

at an incident energy of *24.1 GeV* per nucleon. In this case, the H_0 mass was implied to be approximately *2.093 GeV/c^2*. BNL-AGS experiment 810 [ref. 7.12] claims forty-four possible candidates through $H_0 \to \Sigma^- + p$ channels, with a lifetime of $c\tau$*~10 cm*.

The experimental set-up of E896 was designed to be sensitive to several different H_0 decay modes, corresponding to H_0 lifetimes in the range of *4 cm* (*133 ps*) $\leq c\tau \leq$ *1 m* (*3.3 ns*). The primary detector of the experiment is optimized to track the decay channel $H_0 \to \Sigma^- + p \to n + \pi^- + p$ which has the largest branching fraction (~30%) for an expected lifetime of the H_0 lower than *100 ps*. Other accessible channels in E896 are $H_0 \to \Lambda + p + \pi^-$ (~13%), as well as the strong decay $H_0 \to \Lambda + \Lambda$.

The experimental apparatus designed to measure the different H_0 decays can also efficiently measure other unstable strange particles such as K_s-mesons, Ξ, Λ and $\overline{\Lambda}$. Interesting physics topics which will be studied with these measurements include $\Lambda/\overline{\Lambda}$ production ratios, $\Lambda\Lambda$ and $K_s^o K_s^o$ interferometry, Λ polarization, K_s and Ξ^- production cross sections.

7.1.2 General experiment layout

Figure 7.2 shows the floor view of experiment E896. It consists of two dipole magnets ("sweeper" and "analyzer"), an array of Silicon Drift Detectors (SDDA), the Distributed Drift Chamber (DDC), a neutron detector (MUFFINS), a time of flight wall array (TOF) and beam defining/trigger detectors.

The "sweeper" magnet is a super-conducting magnet capable of providing a *6.2 Tesla* uniform magnetic field in a *15 cm* high, *30 cm* wide and *100 cm* long

volume. Its primary purpose is to deflect all of the many hundreds of primary charged particles that are produced in the reaction away from the main tracking detector the DDC, which is located in the analyzer magnet (1.8 Tesla). The deflection of the charged particles by the sweeper magnet allows a higher acceptance for the H_0 measurement by reducing the background and therefore improving the tracking efficiency in the DDC, under the assumption that the neutral H_0 will not decay before it reaches the DDC.

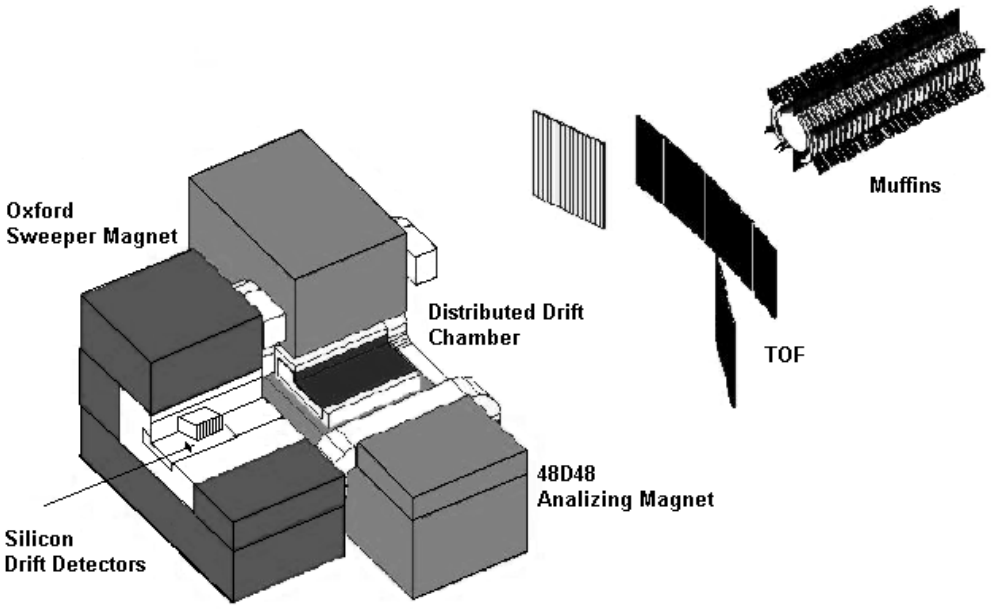

Figure 7.2: *Floor view of the E896 experiment.*

The DDC consists of a contiguous set of 24 modules, each of which is composed of six wire planes, yielding a total of 144 tracking planes. Its design is optimized for short tracks and double-track resolution. A collimator was placed in the front of the DDC, to further reduce the background.

The array of Silicon Drift Detectors (SDDA) is placed inside the "sweeper" magnet, at a short distance from the interaction point (*~5 cm* between the first detector and the target) for charged particle tracking and reconstruction of primary and secondary vertices. It consists of 15 single layers of linear Silicon Drift

Detectors mounted in a telescope configuration. With the SDDA, the acceptance for measuring short-lived particles increased considerably without adding any additional secondary background to the DDC tracking detector. Due to the strong sweeper field, charged particles that leave a signal in the SDDA are not detectable in the DDC. With a coverage in pseudo-rapidity of η=*0.8-1.8* and *20°* in ϕ, the SDDA has high efficiency in measuring short-lived particles such as Λ, $\bar{\Lambda}$ and Ξ^-. Also, it allows the search for the H_0 through measurement of a possible short lifetime weak decay channel $H_0 \rightarrow \Sigma^- + p \rightarrow n + \pi^- + p$. According to some models, the H_0 lifetime could be as short as half the Λ lifetime, in which case it would decay well within the range of the SDDA. Thus, the SDDA H-dibaryon measurement complements the DDC measurement.

7.2 Assembly of the SDDA

7.2.1 Detector wafers

The drift detectors used for the SDDA were chosen using the same selection criteria than for the STAR/SVT (see chapter 4). For the January 1997 beam time, the first beam run of experiment E896, only two detectors were assembled, one STAR-2.7 and one STAR-2.9 prototype. The STAR-2.9 detectors had been just produced for the first time and their characteristics were not completely measured. For that reason, it was decided to place a well characterized STAR-2.7 wafer in front of the STAR2.9 detector. In the E896 April 98 beam time, all 15 detectors assembled for the SDDA were STAR-2.9 prototypes.

Once the probe station tests were completed, the selected wafers were cut on an automated laser station [ref. 7.13] to the proper dimensions. The detectors were then mounted on custom printed circuit boards (see section 7.2.3) along with the corresponding front-end electronics.

7.2.2 Front-end electronics

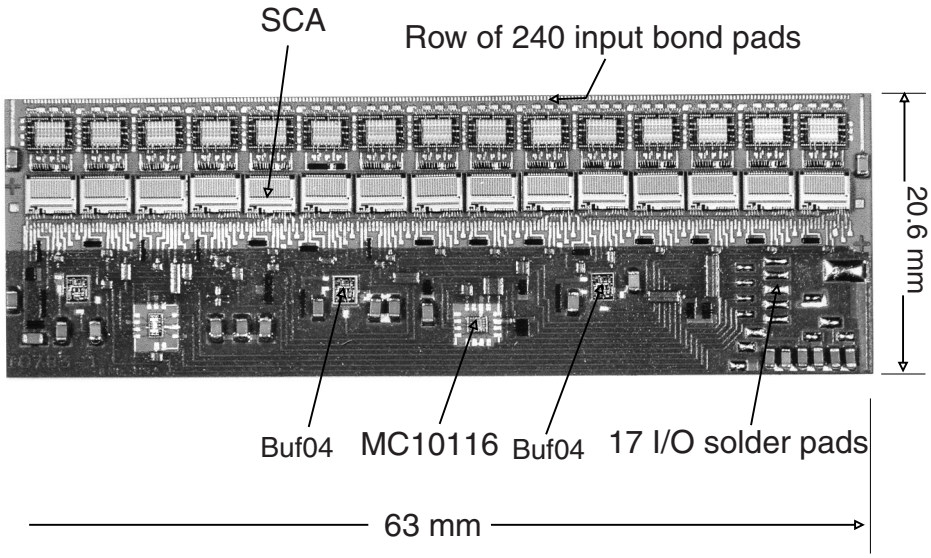

Figure 7.3: *Photograph of a fully assembled hybrid module.*

The front-end electronics consists of pre-amplifier/shaper circuit chips (PASA) and switched capacitor array chips (SCA) mounted on a hybrid carrier. The hybrid carrier is a multi-chip module that combines IC and printed circuit technology on a Beryllia ceramic substrate. Figure 7.3 shows a photograph of the hybrid carrier. Each hybrid contains fifteen 16-channel PASA's and fifteen 16-channel SCA's, capable of reading all 240 anodes from each drift half of the detector. The bipolar PASA circuit was designed in the Instrumentation division of Brookhaven National Laboratory and the CMOS SCA chips was designed at Lawrence Berkley Laboratory, both specifically for the STAR/SVT.

A PASA chip consists of 16 input/output channels of amplifying and shaping integrated circuitry. Each channel is wire bonded to an anode on the detector to measure the incoming electron cloud, equivalent to a current pulse. For an input delta function current, the PASA outputs a bipolar shaped pulse, with a

peaking time of approximately *100 ns*, a width of approximately *50 ns* and a gain factor of *7 μV/electron*.

The SCA is a 16 channel analog memory storage device that receives the shaped signal from the PASA channels. Each SCA channel consists of a circular buffer of 127 capacitors that will sample and store sequentially the signal information from the PASA. The SCA channels are clocked at a frequency of *25 MHz*, which corresponds to a sampling time of *40 ns* per time-bucket.

Once the signal is stored in the SCA capacitors, the voltage on each capacitor is multiplexed onto a common SCA analog output that is transmitted to the readout system for digitization. Each group of five SCA chips with a total of 80 channels is multiplexed into one analog output to a common analog buffer. Therefore, each hybrid module, with 240 readout channels contains three analog output buffers. Additionally, on each hybrid, there are pseudo-ECL level driver circuits to fan out the differential clock and CMOS buffers to drive the control signals to the SCA's.

The power and control-signals for the front-end electronics were provided from the Readout system, which is described later in this chapter (section 7.2.4).

7.2.3 Detector assembly on the PC-board and support structure

Once the detector wafer and the hybrid were tested independently, they were both integrated on a PC-board, as shown in figure 7.4. It is made of G-10 with dimensions of *12cm × 16.6cm*. Each PC-board holds one detector and two hybrid carriers.

To the left of the detector, on both surfaces, there is an external voltage divider (resistor chain) to support the voltage linearity of the detector. Every 10^{th}

cathode on both sides of the detector is wire bonded to a printed circuit trace connected to the external voltage divider. Ultrasonic wedge bonding technique was used with a *25 μm* aluminum wire. Special considerations were taken in the design of the voltage divider. The circuit had to be designed to spread over as large an area as possible to reduce the local heat dissipation, and also to maximize the distances between traces with high voltage differences to avoid voltage breakdowns.

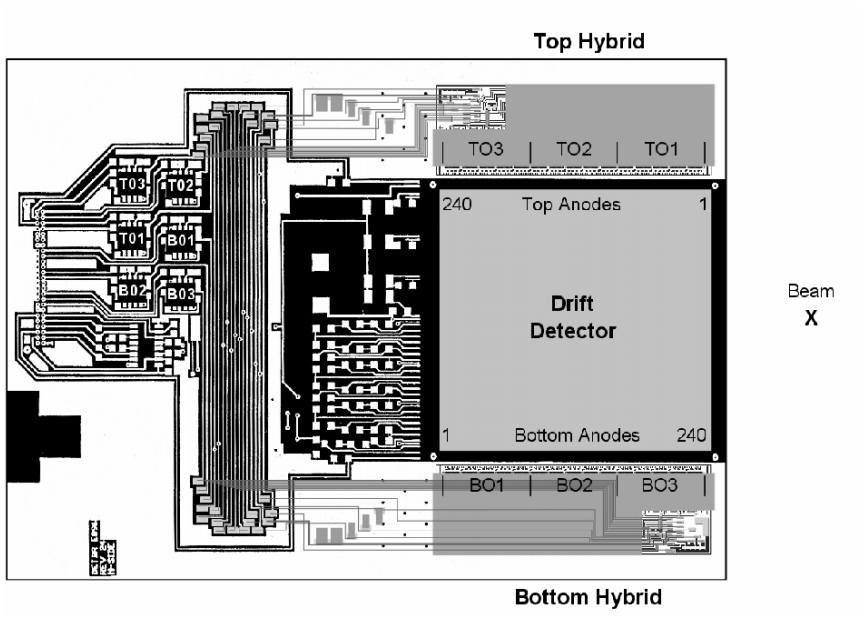

Figure 7.4: *Schematic of the E896 PC-board with the detector and the front-end electronics (hybrids).*

Hybrid carriers were placed on each side of the detector and their bond pads were aligned with the anodes. They were glued onto the PC-boards using a heat conductive epoxy that facilitated the cooling. Each detector anode was connected to an input channel of the PASA through wire bonds. Six analog differential driver stages and one digital differential line receiver were mounted on the surface of the PC-board. Input and output signals were transmitted through an 80-pin card connector, placed on the left edge of the PC-board.

Each component mounted on the PC-board was tested before and after the assembly procedure. A special testing station was used to read the signal from the front-end electronics and test the integrated system. Hybrid measurements, such as noise levels, were taken throughout every step of the assembly procedure. One particular concern was that the additional input capacitance to the PASA due to the anode and the wire bonds could increase the electronic noise. Measurements showed that with the detector biased, i. e. anodes depleted, the noise settled within acceptable limits, below *5 mV* (*~750 electrons*). Some filtering capacitors were added to the power lines to attenuate external noise, such as ground level oscillations.

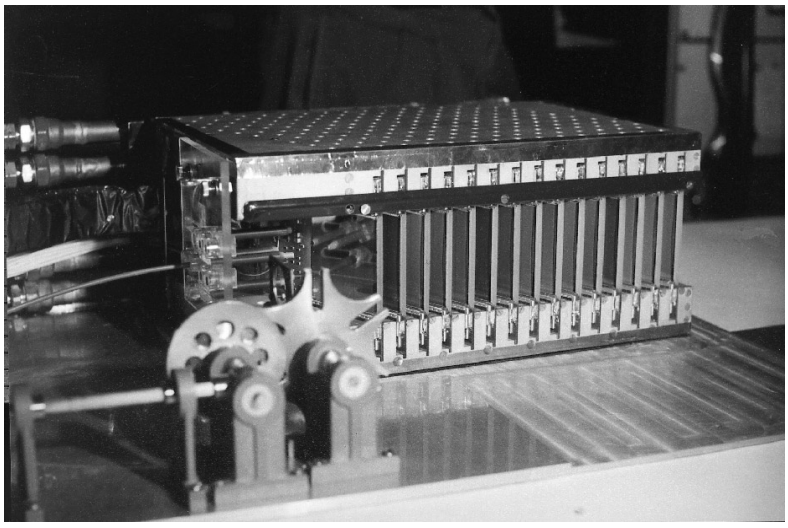

Figure 7.5: *Picture of the Silicon Drift Detector Array (SDDA) assembled for the April 1998 beam run of AGS-BNL experiment 896.*

The PC-boards were held in position by an aluminum support structure that was mounted inside the sweeper magnet. It was designed to hold 15 layers of PC-boards, backed by a water cooling system, mainly to cool the front-end hybrid carriers. Figure 7.5 shows a picture of the Silicon Drift Detector Array (SDDA) assembled with 15 detectors used in the April 1998 data taking beam time.

7.2.4 Readout and Data Acquisition

The readout and data acquisition (DAQ) system used for the SDDA in the experiment E896 is a prototype of the final STAR/SVT system [ref 7.14]. It was developed in a collaboration between the University of Texas, Austin and Brookhaven National Laboratory. Figure 7.6 shows a layout of the Readout and Data Acquisition (DAQ) system.

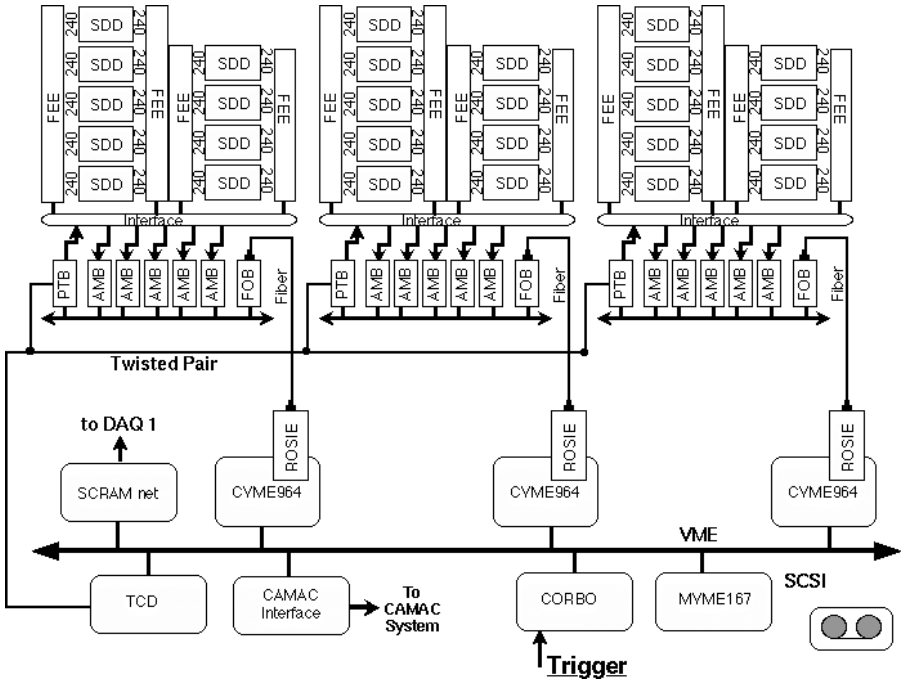

Figure 7.6: *Schematic of the E896-SDDA Readout and DAQ layout.*

The readout system consists of readout boards (RDO) which host the Analog to Digital Converters (ADC's). The data readout sequence reads from SCA to SCA recording the value from the first time-bucket of the 240 anodes of each hybrid, before moving on to the second time-bucket. The signals from the ADCs are sent to the DAQ through an optic fiber link. The DAQ has an optical receiver card specially developed for STAR (ROSIE card). Each Readout system can read up to 18 hybrid carriers, equivalent to 9 detectors.

In the DAQ, the ROSIE receiver cards are mounted on a Cyclone CVME964 card, which contains an Intel 80960 processor. In the STAR/SVT, a data filtering and zero-suppression step will be implemented with a customized Application Specific Integrated Circuits (ASIC) that will reduce the amount of data. For the E896 experiment, no data suppression was used. All the data (240×127 pixels per hybrid) were recorded to magnetic tapes.

To interface with the experiment trigger system, a trigger and "clock" distribution board was developed to control the readout and the DAQ. When an event trigger occurs, the "clock" signals are sent to the front-end electronics to readout the data from the SCA's. The trigger card also sets a "busy" status on the ROSIE board. Only after the whole event is received and stored in the ADC's of the RDO's the event-end signal will change the status of the ROSIE card to call the DAQ processor. While the DAQ is processing the data and writing it to tape, the Readout system is kept in "busy" mode. That ensures that the data in the Readout system cannot be reset before the DAQ write cycle is completed.

The data acquisition rate during the first beam time was on the order of *0.5 Hz*. This rate was limited by the data taping process, which at the time, utilized an Exabyte 8500 tape drive. During the second beam time, a higher data acquisition rate of approximately *2 Hz* was achieved using a MAMMOTH tape drive.

7.3 Beam and data taking

The E896 experiment performed an engineering run in January of 1997 and a data run in April of 1998 using Gold beam with an energy of *11.6 GeV* per nucleon. A Gold target was used with a thickness equivalent to a *10%* interaction length. Empty target events were also interspersed for background study purposes. For the main "physics" events, a "central" trigger cut on the upper 20% of the geometric cross section was applied. Coincidence of two beam counters and a

multiplicity detector that was put in anti-coincidence with a charge detector were used to form the trigger.

During the 1997 engineering run, the sweeper magnet in which the Silicon Drift Detectors were placed generated a magnetic field of *4.7 Tesla*. Only two Silicon Drift Detector planes were assembled and only half of each plane was implemented with front-end-electronics. It was the first time the STAR Silicon Drift Detectors were used together with its front-end-electronics and the readout system in an experimental environment. It was an important integration test for the STAR/SVT project. Also, this beam time provided a unique opportunity to have real experimental data from the Silicon Drift Detectors for the development and refining of the readout and analysis software. During a period of 7 days, more than 65,000 events were recorded with the Silicon Drift Detectors.

In the second beam time, which took place in April of 1998, a setup of 15 planes of fully instrumented detectors was placed in the sweeper magnet which generated a magnetic field of *6.2 Tesla*. About one million events were recorded in 25 days of data taking. We expect to have recorded about $200 \cdot 10^3$ Λ, 400 $\overline{\Lambda}$ and 500 Ξ^- in the SDDA data sample. The H_0-dibaryon yield depends strongly on the model, but optimistic estimates set the number to about 100 candidates.

The 15 PC-boards with detectors and front-end hybrid carriers were held inside the aluminum support structure in vertical orientation, parallel to each other as shown in figure 7.5. The SDDA was fixed on a base plate (called target plate) that also holds the target mechanism and a multiplicity detector positioned behind the SDDA. To avoid electric ground problems and shield against electrical noise, the SDDA was electrically isolated from the aluminum plate. The fully instrumented plate was then positioned inside the sweeper magnet.

The detectors were powered using a Le Croy 1454-HP mainframe power supply. It provided the high voltage to the external resistor chain mounted on the

PC-boards, including the anode focusing voltages. A "slow controls" system was implemented to control and monitor remotely the high-voltage power supply. In addition, it measured other detector parameters such as guard anode currents, and temperature from thermistors mounted on the PC-boards.

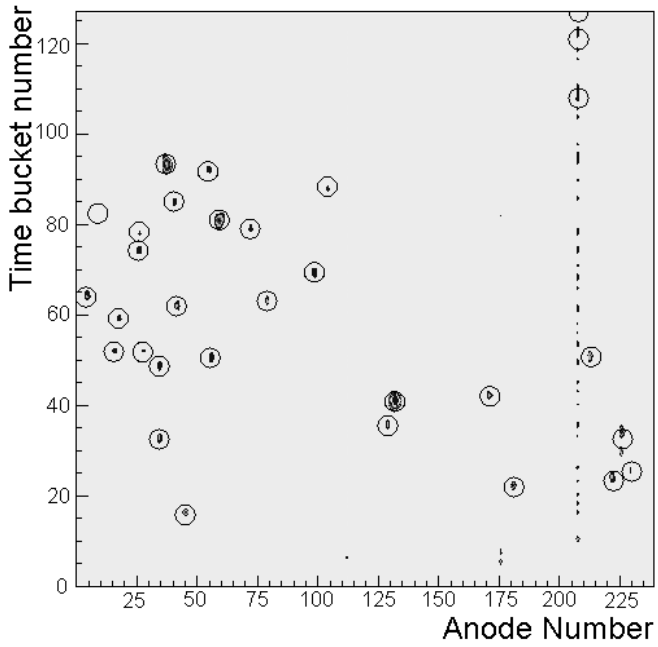

Figure 7.7: *Two-dimensional plot of a half detector, from the online monitoring program.*

During both data taking periods on-line monitoring software was used to view raw events from the detectors, display hits and calculate detector pedestals, noise levels and fluctuations. Figure 7.7 is an example of a two-dimensional plot of the on-line program that shows the readout from one hybrid (half a detector). A simple and fast "hit finder" code was developed to find hit signals using a pedestal subtraction and single threshold method. A circle marks the hits found by the "hit finder". For off-line analysis, a more sophisticated "cluster finder" code was developed to find the hits and their coordinates on the detector. Further descriptions of the analysis code will be given in the next section 7.4.

7.4 Offline analysis overview

The first step of the offline analysis is the "data reduction" or "zero suppression". It contains code to determine the position and energy of each "hit" on the detectors. The "raw" data undergo the following steps during the zero suppression procedure: pedestal subtraction, noise filtering, cluster finding and cluster analysis. Each of these steps will be described in the following sections.

Once each hit position is determined, the next stage of the offline analysis consists of determining the particle trajectories and calculate their momenta. The first step consists of aligning the coordinates from different detector layers to the same reference alignment. That is accomplished by analyzing straight tracks of high momentum particles that have traversed several detector layers. Also, during the April 98 beam time, some events were measured with the magnet "off", which contained straight tracks for alignment purposes. Once the detector coordinates are aligned, hits from different detector layers need to be grouped into track candidates. The hit "grouping" code starts with hits on the first detector layer and searches for hits on the next detector layer near the projected coordinate, calculated considering a straight track from the previous layer. The search radius can be changed according to the momentum range, therefore, an iterative process can be performed starting with high momentum particle trajectories (straight tracks) down to lower momentum tracks that will have a bigger trajectory curvature. By excluding identified tracks the efficiency in determining correct tracks improves considerably, especially in relatively high hit density detector areas. Once the hits are grouped together, a circular fit is performed and the particle momentum is calculated. In a homogeneous dipole field a simple circle fit is sufficient to determine the momenta.

Limited particle identification is possible for low momentum particles using dE/dx techniques. Energy deposition measurements from different detector layers

improve the energy resolution for the dE/dx spectrum. Particle identification can contribute considerably to background subtraction.

Once the particle momentum is determined, different analysis techniques are used according to the physics goals. The analysis results include kinetic spectra, invariant mass spectra, two particle correlation functions, yield and ratios of certain particle species. The invariant mass spectrum is calculated to identify particles through their decay channels. For example for the charged decay branch of the Λ ($\Lambda \to p + \pi$), the invariant mass is given by:

$$m_{\Lambda} = \frac{1}{c^2}\sqrt{\left(E_p + E_{\pi}\right)^2 - \left(p_p + p_{\pi}\right)^2 c^2} \qquad \textbf{(7.1)}$$

In the Λ analysis, differently charged pairs of emitted particles are connected under the assumption of having m_{Λ}=115 MeV. The background is based on wrong combination of positive and negative charges, and can be estimated by combining negative and positive charges from different events (event mixing). For the measurement of the H_0 in the SDDA, a characteristic topology of the $H_0 \to \Sigma^- + p$ decay channel helps to reduce the background, where the subsequent decay of $\Sigma^- \to n + \pi^-$ leads to a "tertiary" vertex which is characterized by a "kink" due to the emission of the non-detectable neutron.

In addition to the data analysis, heavy-ion collision event generator codes were used to simulate the reaction and its produced particles. For experiment E896, mainly two different event generators were used: ARC [ref. 7.16] and RQMD [ref. 7.17]. Both ARC, which stands for "A Relativistic Cascade", and RQMD, which stands for Relativistic Quantum Molecular Dynamics, are Monte Carlo simulation codes that describe relativistic heavy-ion collisions by employing a string fragmentation approach. Hadrons are produced by string fragmentation as soon as the effective string tension in a quark string exceeds a certain value. The

hadrons subsequently interact via a hadron cascade in which the interaction cross sections are defined by measurement of free nucleon-nucleon, nucleon-meson and meson-meson cross sections. Hadronic resonances are also included, which leads to a more reliable description of the interactions. Comparison to past AGS experiments [ref. 7.21] show that the global observables as well as the specific observables for the main particles (p, K, π) are well described by ARC and RQMD.

The subsequent propagation of the particles, secondary reactions and particle decays were calculated using a simulation package called GEANT [ref. 7.22], developed by the CERN computing center. GEANT accepts the events generated by ARC and RQMD and it transports the particles through the various regions of the experimental setup, considering interactions with matter, magnetic fields and all other physical effects according to the nature of the particles. It provides the particle trajectories and the detector response (hits). Detector performance can be verified by comparing the experimental results with the GEANT output. From this comparison, the detector geometrical acceptance and the efficiency can be determined for corrections in the cross section calculations. A third simulation stage called "slow simulator" considers the GEANT "hits" output and simulates the actual detector response. The "slow simulator" package considers the electron cloud drift, the front-end electronics response, including noise effects and outputs data in the same format as the real data acquisition. By combining all these packages, a complete simulation of the event can be performed.

The offline analysis code is structured in a modular way such that each step of the data reduction is an independent, stand-alone code. The analysis code development is a collaborative effort between the members of the SVT-E896 groups from Wayne State University, the Ohio State University, the University of Texas and Brookhaven National Laboratory [ref. 7.15].

In this thesis, the first part of the offline analysis, the data reduction, is described. Other parts of the analysis code are still in development and will be described in future documents.

7.4.1 Pedestal subtraction

The signal from each anode is read out through an array of 127 capacitors of the SCA. The detector output can be seen as a pixelized matrix of ADC values where each "pixel" corresponds to a single time-bucket of a single anode. For each pixel, the ADC value can be between 0 and 1024 channels, but a common ADC offset is set for all pixels in the detector. This offset corresponds to the pixel "pedestal". Ideally, all the pixels would have the same pedestal value, resulting in a "flat" ADC distribution in the case of no hits on the detector. However, the pedestal values vary with the PASA gain, thus it changes from anode to anode. Also, within the same SCA channel (for the same anode), different capacitors can have different pedestal values, however this variation is expected to be small. Most of the variation is expected due to different PASA gains.

The pedestal of each pixel should not vary in time, thus if the pedestal of each pixel is known, it can be subtracted in every event. Pedestal values are calculated for each pixel averaging its ADC value over the course of a data taking run, approximately 1000 events per run. Figure 7.8 shows the ADC value for a single pixel plotted as a function of the event number. This plot shows that the pedestal is indeed stable in time, except for noise contributions. In some events, a group of pixels can have an ADC value different from its pedestal value due to a "hit". However the hit occupancy is sufficiently low such that the effect of hits on specific pixels is negligible for the averaging procedure.

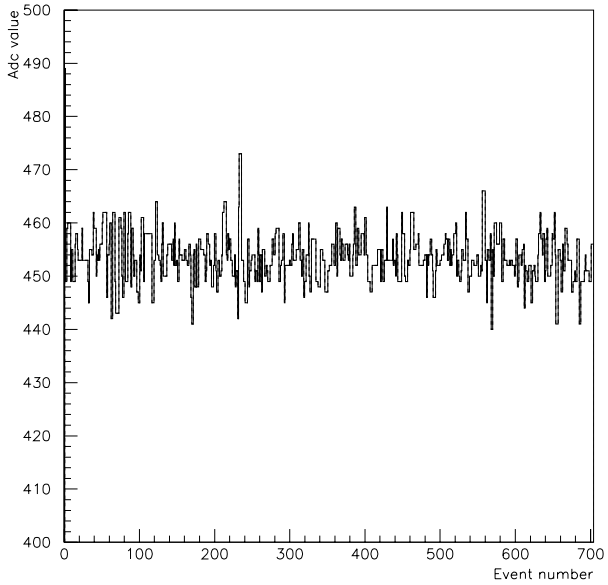

Figure 7.8: *ADC values measured in a single anode through the course of a data taking run with approximately 700 events.*

Due to the fact that the SCA is a circular buffer of capacitors continually processing, and that the event trigger can occur at any time during the cycle, the first time-bucket number (time of hit with respect to time of collision plus trigger generation time) does not always correspond to the same actual capacitor of the SCA. For that reason, to calculate the exact pedestal value, it is necessary to determine the real capacitor number for each time bucket, on an event by event basis. However, considering that the pedestal variation between capacitors of the same SCA channel is relatively small, it is sufficient to calculate the time-bucket pedestal without mapping to the real capacitor number. In the SVT, the capacitor number of the first time-bucket will be stored, thus it will be possible to correlate the time-bucket number with the capacitor number and subtract the pedestal equivalent to each capacitor.

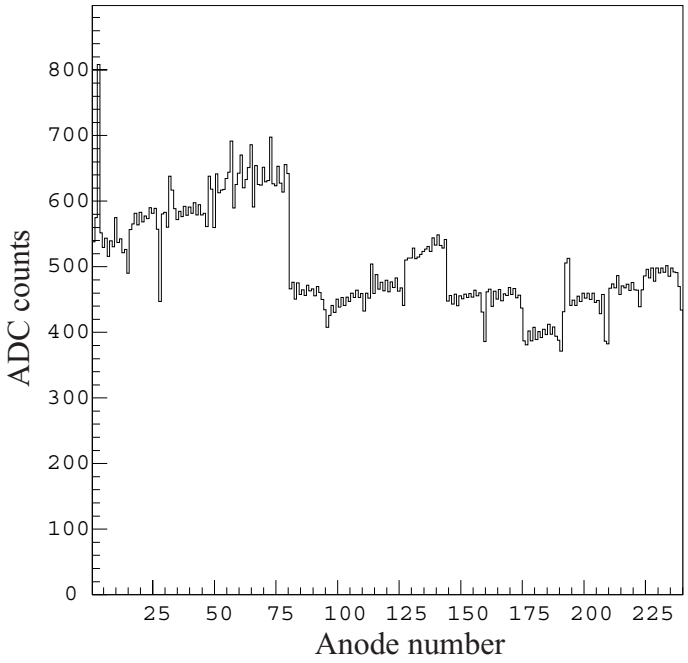

Figure 7.9: *Pedestal values from one time-bucket, plotted as a function of the anode number.*

Figure 7.9 shows a typical pedestal plot with pedestal values measured for one time-bucket, as a function of the anode number. As expected, the pedestal levels vary from PASA to PASA, depicted by the step pattern between sets of 16 anodes.

Once the pedestal for each pixel is calculated, it is subtracted on an event by event basis. In each event, the mean deviation of all pixel values from its pedestal is defined as the noise of the detector. In the January 1997 data, the calculated mean value of the noise distribution is around *10 mV*, a factor of two larger than the typical noise measured with the detectors in the bench tests. In the April 1998 data, the better shielding and grounding led to a considerable reduction in the detector noise, around *4.5 mV*, almost reaching the same level as the intrinsic noise measured in the bench tests.

7.4.2 Noise filtering (common mode noise subtraction)

Figure 7.10 shows the ADC values from one event, averaged over 240 anodes, projected in the time-bucket direction, after the pedestal subtraction. An oscillation common to all anodes in the same event is observed. It does not appear in the pedestal because the phase of this noise with respect to the trigger (time-bucket zero) changes from event to event. Since it is common across the anodes, it is defined as a "common mode noise". The oscillation pattern indicates that the noise is most likely generated by some correlated noise pick-up.

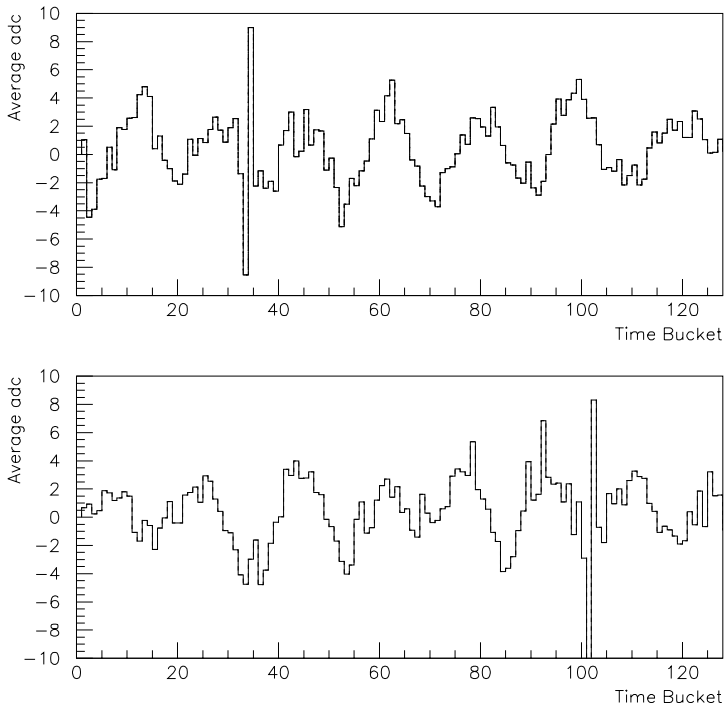

Figure 7.10: *Averaged over 240 anodes ADC values as a function of the time-bucket number for one event, after pedestal subtraction.*

In both data taking runs, January 1997 and April 1998, common mode noise was observed, however in the latter, due to better shielding and grounding of the detector and electronics, the amplitude of the oscillation was smaller. The exact source of the noise was not determined, though its frequency, which is between *1*

MHz and *2 MHz*, might indicate generation by an external source like a local AM radio station or some magnet control switch.

The common mode noise is eliminated by subtracting the average value of 240 pixels for each time-bucket, on an event by event basis. Limits are placed on the ADC values in the calculation of the average in order to minimize the impact of actual particle hits in the time-bucket average value.

In summary, the "raw data" undergos two "subtraction" steps before the hit cluster finder code. First, a pedestal value is subtracted from each pixel, based on a pixel pedestal that was calculated averaging the pixel ADC value over several events. Then, an averaged value of 240 pixels for each time-bucket is subtracted from each pixel to deduct the common mode noise.

7.4.3 Cluster finding and zero suppression

Once the pedestal and the common mode noise are subtracted, the analysis program proceeds to the "zero suppression" algorithm. This algorithm searches for hit clusters and stores a certain number of pixels around the cluster. To determine a cluster, it considers the following requirements:

- **High threshold:** The algorithm scans through all the pixels in the detector looking for pixels above a user defined high threshold. A typical value used for this threshold was *12 mV*, which corresponds to about twice the average noise level measured in each pixel. Once, a high pixel is found, it is considered as a possible hit candidate.

- **Low threshold:** The algorithm searches the neighboring pixels of the candidate pixels that have passed the high threshold requirement, and counts

how many neighboring pixels are above the low threshold value. A typical value used for the low threshold was *10 mV*.

- **Minimum Neighbors:** For a hit candidate to be considered as a hit cluster, a minimum number of neighboring pixels has to be above the low threshold. Typically it was required that at least 4 out of 8 neighboring pixels were above the low *10 mV* threshold.

Once the cluster is found, additional pixels around the candidate pixels are saved to record the entire cluster. In the anode direction, two neighboring pixels in both directions are saved. In the drift time direction, the algorithm considers the bipolar signal shape and looks for the signal undershoot. A running average of every two pixels, starting from the cluster peak is calculated searching for negative ADC counts, which would correspond to the signal undershoot. The cluster size in the drift direction is defined as twice the distance between the peak and the undershoot.

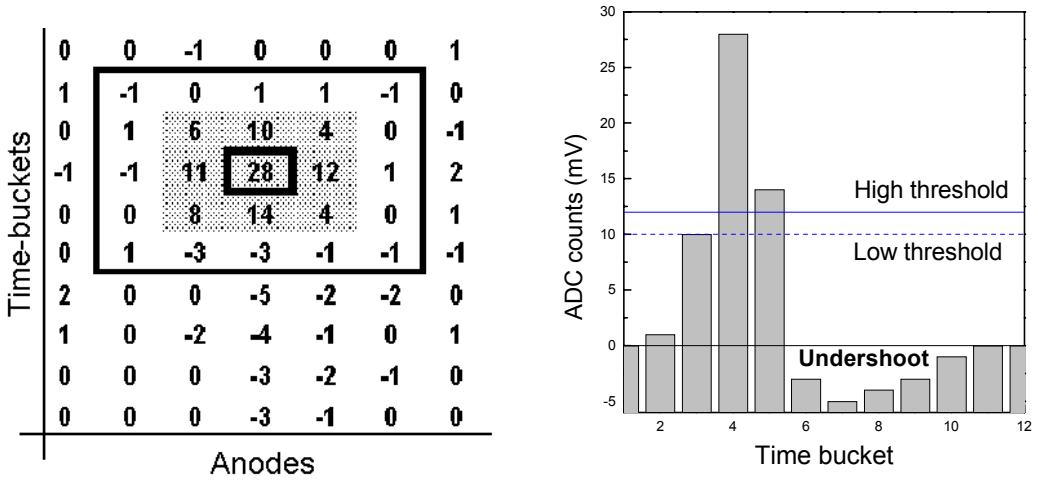

Figure 7.11: *(a) Map of pixel ADC values to illustrate the cluster finding algorithm. (b) Time projection of the highest pixel anode, with the high and low threshold indicated by the horizontal lines.*

Figure 7.11 illustrates an example of a hit cluster and the result of the "cluster finder" algorithm. Three candidate pixels above the high threshold are found with ADC values 28, 14 and 12. Checking the neighboring cathodes, the code determines that only the pixel with ADC count 28 has the minimum number of neighboring pixels with values above the lower threshold. Starting from the highest pixel, the algorithm follows the time-bucket sequence searching for the signal undershoot. Once, the running average becomes negative, the algorithm defines the size of the cluster as shown in figure 7.11(a).

The efficiency of finding good hits and rejecting false clusters depends greatly on the parameters used in the zero suppression algorithm. Careful studies varying these parameters were performed and led to an optimized algorithm [ref. 7.18].

7.4.4 Cluster analyzer and hit position determination

Figure 7.12 shows an example of a hit cluster, in a two-dimensional plot. The area shown is larger than the area that is stored by the "cluster finder" algorithm. Once the hit cluster is stored, the next step is to determine the position, size and ADC sum of the cluster. Two approaches were developed to obtain those parameters. The first approach is based on a fit of the signal shape in both directions, transverse and longitudinal. Although this method is more accurate, it is very time consuming, and to analyze a large amount of data (more than a total of 1 billion hits from both E896 runs) a faster method is required. The second method is a simple moment analysis of the cluster, which determines the cluster position by considering the ADC counts of each pixel. Both approaches are discussed in the following paragraphs.

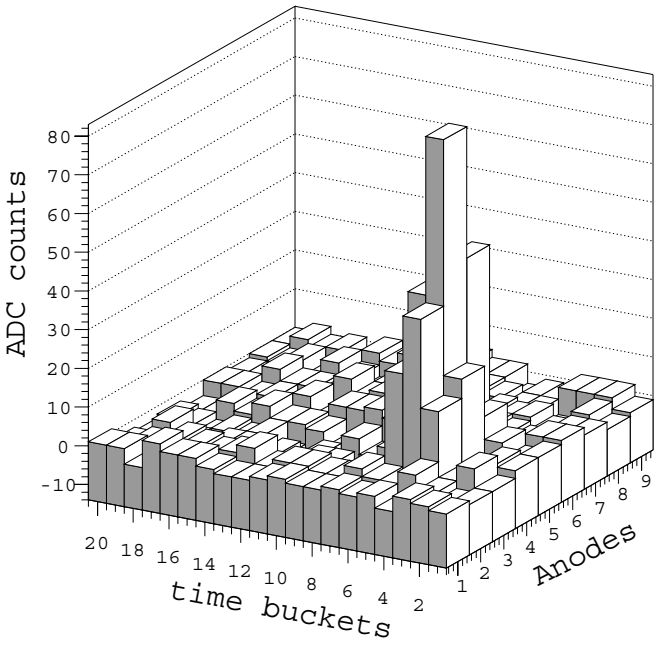

Figure 7.12: *2 dimensional lego plot of a particle hit cluster.*

7.4.4.1 Moment analysis

The moment analysis method consists of determining the position of the cluster center by performing a weighted average of the cluster distribution considering the ADC counts of each pixel.

The zeroth moment of the cluster distribution corresponds to the total sum of the ADC values from all pixels.

$$Q = \sum_{i,j} u_{i,j} \qquad \text{for } u_{i,j} \geq u_{min}. \tag{7.2}$$

where "$u_{i,j}$" is the ADC value of the pixels located at anode "i" and time-bucket "j". A minimum threshold "u_{min}" is used to eliminate negative ADC values of the signal undershoot created by the PASA response function. To consider only the positive portion of the bipolar signal "u_{min}" was set to a value close to zero, *-5 mV*.

It was not set exactly to zero to account for pedestal fluctuations due to noise, which are around $\pm 5\ mV$.

The first moment of the distribution determines the centroid position of the cluster.

$$X \approx m_1 = \frac{\sum_{i,j} x_i \cdot u_{i,j}}{\sum_{i,j} u_{i,j}} \qquad \text{for } u_{i,j} \geq u_{min}. \tag{7.3}$$
$$Y \approx m_2 = \frac{\sum_{i,j} y_j \cdot u_{i,j}}{\sum_{i,j} u_{i,j}}$$

where "x_i" is the pixel position in the anode direction and "y_j" is the pixel position in the drift-direction. "X" and "Y" are the coordinates of the electron cloud in the transverse (anode) and longitudinal (drift) directions, respectively. The second moment provides information on the size of the cluster in both dimensions.

$$m_{11} = \frac{\sum_{i,j} x_i^2 \cdot u_{i,j}}{\sum_{i,j} u_{i,j}} - m_1^2 \tag{7.4}$$
$$m_{12} = \frac{\sum_{i,j} \left(x_i \cdot y_j\right) \cdot u_{i,j}}{\sum_{i,j} u_{i,j}} - m_1 \cdot m_2 \qquad \text{for } u_{i,j} \geq u_{min}.$$
$$m_{22} = \frac{\sum_{i,j} y_j^2 \cdot u_{i,j}}{\sum_{i,j} u_{i,j}} - m_2^2$$

"m_{11}" and "m_{22}" correspond to the RMS of the cluster distribution in the transverse and longitudinal directions, respectively. To correlate these parameters to the actual size of the electron cloud it is necessary to correct the width in the longitudinal direction by de-convoluting the gaussian width from the PASA response function output.

For single hits, the moment analysis provides reliable information of the cluster position and size. However, hits positioned closely to each other (double hits) are more difficult to analyze through this method. Special double hit cluster analyzer codes are being developed separately. In E896, as well as STAR, the hit occupancy is sufficiently low so that in general, hit merging is not a major concern. However, to detect secondary vertices, double hit resolution is a very important parameter. More detailed studies of double hit resolution in Silicon Drift Detectors can be found in references 7.19 and 7.20.

7.4.4.2 Cluster fitting procedure

As mentioned earlier, the cluster fitting procedure is a more accurate way to determine the cluster position, however, it takes a considerable amount of processing time. Thus it was used only on a small subset of the data to compare its results with the results from the moment analysis procedure.

In the transverse direction (parallel to the anodes), the shape of the electron cloud is approximated by a gaussian. In the longitudinal direction (drift direction), the electron cloud gaussian is convoluted by the pre-amplifier/shaper output response function. The Laplace transform of an input delta function to the PASA output is:

$$F_{PASA}(s) \propto \frac{s}{(s+1/\tau_{short})^5 \cdot (s+1/\tau_{long})} \qquad \textbf{(7.5)}$$

where τ_{short} and τ_{long} are two time constants that determine the rise time and the undershoot of the bipolar signal. Exact values of these parameters depend on specific details of the PASA circuit design. Based on the original PASA design, the nominal values of these parameters are: $\tau_{short} \approx 11.5\ ns$ and $\tau_{long} \approx 500\ ns$.

Figure 7.13 shows the cross section of the signal shown in figure 7.12 in the longitudinal and transverse direction, respectively. The dashed curves represent the fit in both directions, which show good agreement with the experimental data. In the drift direction, the data was described by the PASA response function convoluted with a Gaussian distribution, where the two time constants, τ_{short} and τ_{long}, were treated as free parameters of the fit.

The comparison between the fitting procedure and the moment analysis was performed for different cluster sizes and clusters from different drift distances. In general the results from the two methods have shown good agreement. A slight systematic offset was noted between the position in the drift direction calculated by the two methods. This difference can be attributed to the shape of the bipolar signal, which is not sufficiently considered in the moment analysis. However, any artificial offset generated by the cluster analysis code is cancelled out with the drift calibration and the relative wafer alignment.

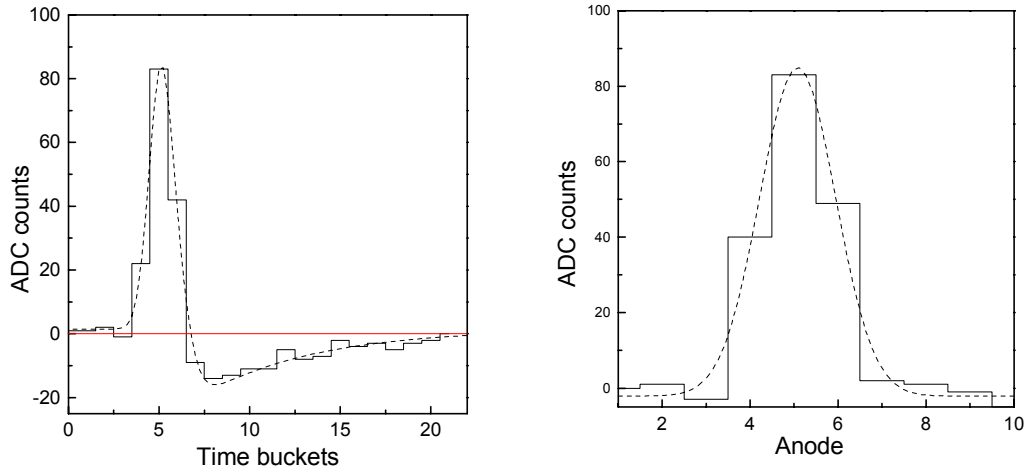

Figure 7.13: *Signal shape in (a) the drift direction and (b) in the transverse direction. The dashed lines represent fitted curves (a) with the PASA response function convoluted with a gaussian distribution and (b) with a gaussian distribution.*